water

MDPI

Article

Mathematical Approach for Directly Solving Air–Water Interfaces in Water Emptying Processes

Dalia M. Bonilla-Correa [1], Oscar E. Coronado-Hernández [2,*], Alfonso Arrieta-Pastrana [2], Vicente S. Fuertes-Miquel [3,*], Modesto Pérez-Sánchez [3] and Helena M. Ramos [4]

[1] Facultad de Ciencias Exactas y Naturales, Universidad de Cartagena, Cartagena 130001, Colombia; dbonillac@unicartagena.edu.co
[2] Instituto de Hidráulica y Saneamiento Ambiental, Universidad de Cartagena, Cartagena 130001, Colombia
[3] Departamento de Ingeniería Hidráulica y Medio Ambiente, Universitat Politècnica de València, 46022 Valencia, Spain
[4] Civil Engineering, Architecture and Environment Department (CERIS), Instituto Superior Técnico, University of Lisbon, 1049-001 Lisbon, Portugal; helena.ramos@tecnico.ulisboa.pt
* Correspondence: ocoronadoh@unicartagena.edu.co (O.E.C.-H.); vfuertes@upv.es (V.S.F.-M.)

Abstract: Emptying processes are operations frequently required in hydraulic installations by water utilities. These processes can result in drops to sub-atmospheric pressure pulses, which may lead to pipeline collapse depending on soil characteristics and the stiffness of a pipe class. One-dimensional mathematical models and 3D computational fluid dynamics (CFD) simulations have been employed to analyse the behaviour of the air–water interface during these events. The numerical resolution of these models is challenging, as 1D models necessitate solving a system of algebraic differential equations. At the same time, 3D CFD simulations can take months to complete depending on the characteristics of the pipeline. This presents a mathematical approach for directly solving air–water interactions in emptying processes involving entrapped air, providing a predictive tool for water utilities. The proposed mathematical approach enables water utilities to predict emptying operations in water pipelines without needing 2D/3D CFD simulations or the resolution of a differential algebraic equations system (1D model). A practical application is demonstrated in a case study of a 350 m long pipe with an internal diameter of 350 mm, investigating the influence of air pocket size, friction factor, polytropic coefficient, pipe diameter, resistance coefficient, and pipe slope. The mathematical approach is validated using an experimental facility that is 7.36 m long, comparing it with 1D mathematical models and 3D CFD simulations. The results confirm that the derived mathematical expression effectively predicts emptying operations in single water installations.

Keywords: emptying processes; mathematical approach; Simpson's 1/3 rule; transient event; trapped air; water distribution networks

Citation: Bonilla-Correa, D.M.; Coronado-Hernández, O.E.; Arrieta-Pastrana, A.; Fuertes-Miquel, V.S.; Pérez-Sánchez, M.; Ramos, H.M. Mathematical Approach for Directly Solving Air–Water Interfaces in Water Emptying Processes. *Water* **2024**, *16*, 3203. https://doi.org/10.3390/w16223203

Academic Editor: Anargiros I. Delis

Received: 3 October 2024
Revised: 31 October 2024
Accepted: 5 November 2024
Published: 8 November 2024

1. Introduction

The study of water emptying processes in pressurised pipelines has received limited attention from researchers worldwide, although water utilities routinely conduct this operation [1]. The accurate prediction of emptying processes is crucial to prevent pipeline collapses, as sub-atmospheric pressure pulses may develop during transient events depending on soil conditions and pipe stiffness. An efficient emptying process should ensure that the pipeline is free of air pockets, as large air pockets are recommended before initiating filling operations. This is because more oversized air pockets tend to lower air pocket pressures, which helps mitigate the risk of pipeline failure due to peak pressures. Moreover, these procedures are vital for expelling sediments and minimising issues related to pipe corrosion.

Water utilities should perform this operation to achieve appropriate emptying times and restore the regular operation of water installations as swiftly as possible. In developing

countries, frequent interruptions in water services often occur due to pipeline failures, leaving many communities without access to a reliable water supply.

The emptying process modelling involves multiphase flows (air and water), which should be simulated using thermodynamics and hydraulic formulations. Tijsseling et al. (2016) [2] proposed a 1D model for predicting emptying processes considering a stratified air–water interaction based on a holdup coefficient, which has been experimentally validated [3]. Coronado-Hernández et al. (2018) [4] and Fuertes-Miquel et al. (2019) [1] proposed a 1D mathematical model for analysing emptying operations using pressurised air in combination with a piston flow approach using experimental measurements during the validation model stage. These formulations are based on physical equations considering the rigid water model, a perpendicular air–water interface, and the polytropic law for the air phase, which can be applied for single and irregular profile water installations. When air valves are installed, the air valve characterisation and mass balance equations must be considered. The air balance is composed of air pocket density mixing with the air density in normal conditions. Chen et al. (2024) [5] presented a dataset of laboratory experiments in a large-scale PVC pipeline 275.2 m long with a diameter of 0.25 m, which presents inlet, bridge, and horizontal branches for studying emptying processes.

The 3D computational fluid dynamics (CFD) model allows for the numerical resolution of Navier–Stokes partial differential equations describing fluid behaviour. This technique predicts fluid movement within water installations, including two phases (water and air) [6]. In practise, CFD models are widely accepted by the scientific community as a reliable means of solving the Navier–Stokes equations, as well as the continuity and energy formulations [7–9]. Because of the computational power, one can use CFD quickly and effectively. Another essential feature of CFD models is that their solutions can be as precise as prototype models. Liu et al. (2019) [10] have investigated the emptying operation of an oil pipeline with a complex longitudinal profile, analysing air–water behaviour through 3D simulations using OLGA v7.0 software. Additionally, a 3D analysis of emptying processes was conducted to capture backflow air, employing OpenFOAM software in an experimental facility measuring 4.36 m long. The PVoF model was used with a two-equation turbulence model for the simulation [11].

Currently, the literature outlines two main approaches for solving emptying processes; (i) for 1D models, numerical methods such as Runge–Kutta or Rosenbrock can be implemented using solvers from computational packages like Matlab R2024b [12] and Octave 7.0 [13], among others, and (ii) for 3D CFD models, software packages such as Ansys 2024 R2 [14], OpenFOAM v2012 [15], OLGA 7.0 [10], Flow-3D v12.0 [16], and STAR-CCM+ 2402 [17] are commonly used. The numerical resolution of 1D models necessitates a system of equations that must be carefully integrated to solve the complex differential equations. Three-dimensional CFD models require significant computational times, with simulations of actual pipelines potentially taking several months to complete. In summary, the computation of the main hydraulic and thermodynamic behaviours of emptying processes have been addressed using 2D/3D CFD [11,18] models or applying a differential algebraic equations system [1,2].

This research presents a mathematical approach for directly solving air–water interaction in water emptying processes with entrapped air based on a one-dimensional formulation of the rigid water model, piston flow, and the polytropic law. The system, composed of differential algebraic equations proposed by the authors in previous publications, has been solved numerically and analytically to provide a solution applicable to water utilities for simulating these operations. The approach accounts for an instantaneous valve opening manoeuvre. A practical application to an extensive pipeline is demonstrated, offering a much faster solution than those produced by 3D CFD models. Furthermore, the proposed method is validated through experimental measurements and compared with 1D and 3D CFD models, demonstrating good accuracy in predicting this biphasic transient event.

2. Material and Methods

2.1. One-Dimensional Mathematical Model

The authors have investigated the transient behaviour of water emptying processes in pipelines in references [1,4]. These processes commence with assuming the pipes are initially filled with water. The entrapped air pocket expands upon opening the regulating valves, decreasing air pocket pressure. Typically, the initial air pocket is assumed to be at atmospheric pressure, and sub-atmospheric conditions are reached during these events. The current mathematical model, consisting of differential algebraic equations, was developed by the authors in earlier publications as follows:

$$\frac{dL}{dt} = -v \tag{1}$$

$$\frac{dv}{dt} = \frac{p_1^* - p_{atm}^*}{\rho L} + g\sin\theta - \frac{f}{2D}v|v| - \frac{R_v g A^2}{L}v|v| \tag{2}$$

$$p_1^* = \frac{p_{1,0}^* x_0^k}{(L_T - L)^k} \tag{3}$$

where p_1^* = air pocket pressure; v = water velocity; L = length of the water emptying column; p_{atm}^* = atmospheric pressure; ρ = water density; g = gravitational acceleration; g = friction factor; θ = pipe slope (rad); A = cross-sectional area of pipe; R_v = resistance coefficient; D = internal pipe diameter; L_T = total pipe length; and k = polytropic coefficient.

The initial conditions of the system are given by $v_0 = 0$, $L_0 = L_T - x_0$, and $p_{1,0}^* = p_{atm}^*$ = 101,325 Pa. The subscript 0 indicates an initial condition of analysed variables.

Figure 1 illustrates the scheme of an emptying process in a single pipeline with entrapped air. The system starts at rest with zero water velocity (Figure 1a). Subsequently, when a regulating valve is opened, the emptying process begins, as depicted in Figure 1b. The system again reaches zero water velocity at the end of the biphasic transient event.

2.2. Proposed Mathematical Approach

This section shows the proposed model developed in this research. The model is based on the following assumptions: (i) water movement is described by the Euler equation; (ii) the air–water interface is considered perpendicular to the main direction of a pipeline; (iii) the friction factor is constant during the transient event; (iv) the air phase follows the polytropic law; and (v) the model applies to single water installations with a sufficient pipe slope.

The 1D mathematical model, consisting of Equations (1)–(3), can be rearranged to eliminate dependence on time t.

By substituting Equation (3) into Equation (2), the system of differential equations can be expressed by Equations (1) and (4).

$$\frac{dv}{dt} = \frac{p_{1,0}^* x_0^k}{\rho L(L_T - L)^k} - \frac{p_{atm}^*}{\rho L} + g\sin\theta - \frac{f}{2D}v|v| - \frac{R_v g A^2}{L}v|v| \tag{4}$$

The system comprising Equations (1) and (4) is autonomous [19]; thus, its numerical solution can be carried out in the vL plane by tracking its trajectory. The trajectory consists of points $(L(t), v(t))$, which satisfy Equations (1) and (4). The system can be simplified as follows:

$$\frac{dv}{dL} = \frac{\frac{dv}{dt}}{\frac{dL}{dt}} = \frac{\frac{p_{1,0}^* x_0^k}{\rho L(L_T - L)^k} - \frac{p_{atm}^*}{\rho L} + g\sin\theta - \frac{f}{2D}v|v| - \frac{R_v g A^2}{L}v|v|}{-v} \tag{5}$$

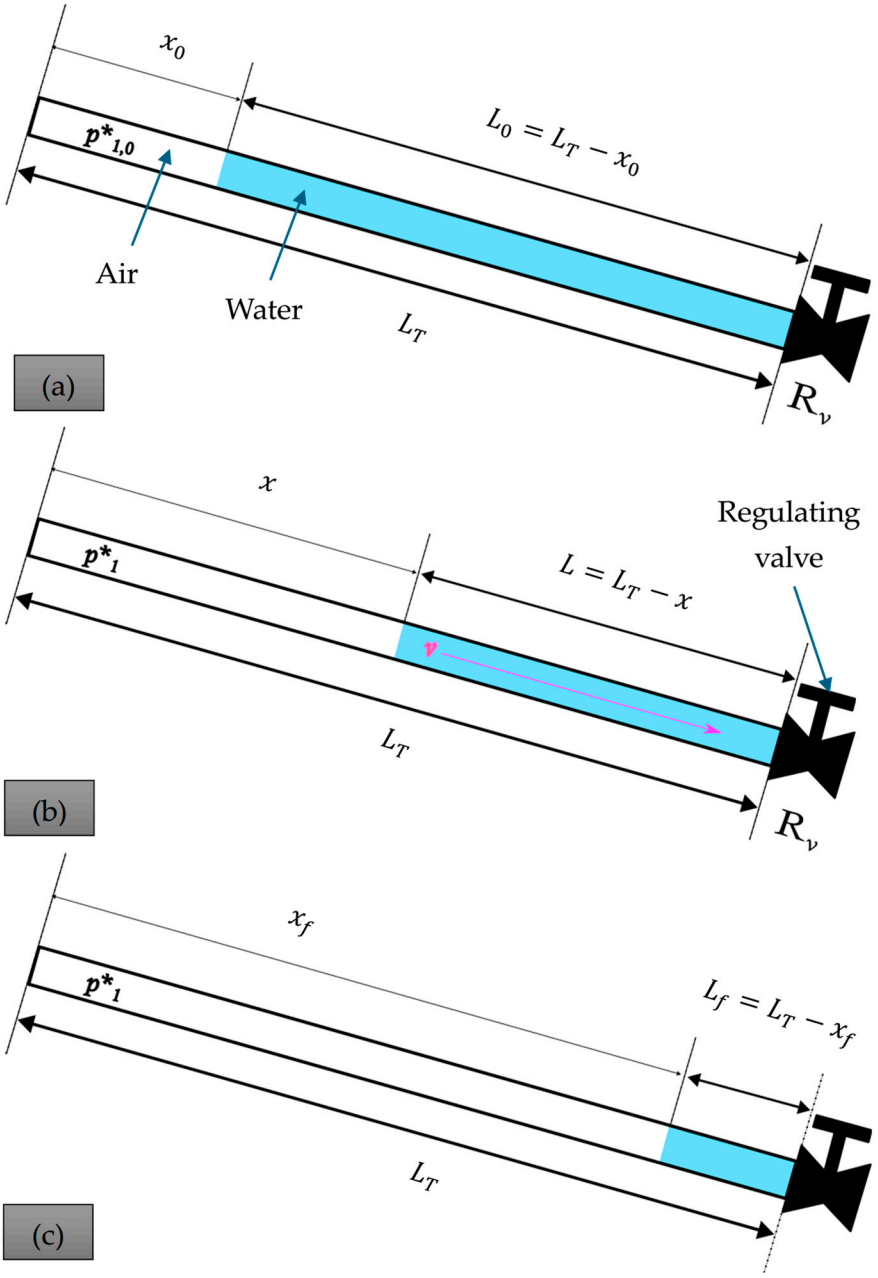

Figure 1. Scheme of water emptying process: (**a**) initial condition, (**b**) intermediate position, and (**c**) final position.

Considering Equation (5), it is possible to compute $\frac{dv}{dL}$. Equation (5) is a single first-order linear differential equation, where L is the independent variable and v is a function of L with no dependence on t. From Equation (5),

$$-v\frac{dv}{dL} = \frac{p^*_{1,0}x_0^k}{\rho L(L_T - L)^k} - \frac{p^*_{atm}}{\rho L} + g\sin\theta - \frac{f}{2D}v|v| - \frac{R_v g A^2}{L}v|v| \quad (6)$$

Multiplying Equation (6) by 2, then

$$2v\frac{dv}{dL} = \frac{-2p^*_{1,0}x_0^k}{\rho L(L_T - L)^k} + \frac{2p^*_{atm}}{\rho L} - 2gsin\theta + \frac{f}{D}v|v| + \frac{2R_v g A^2}{L}v|v| \quad (7)$$

Since $\frac{d(v^2)}{dL} = 2v\frac{dv}{dL}$ and considering the region with the lowest values of sub-atmospheric pressure pulses (where $v \geq 0$), then

$$\frac{d(v^2)}{dL} = \frac{-2p^*_{1,0}x_0^k}{\rho L(L_T - L)^k} + \frac{2p^*_{atm}}{\rho L} - 2gsin\theta + \frac{f}{D}v^2 + \frac{2R_v g A^2}{L}v^2 \tag{8}$$

By defining the auxiliary variable z as v^2, Equation (8) can be expressed in terms of z as follows:

$$\frac{d(z)}{dL} - \left(\frac{f}{D} + \frac{2R_v g A^2}{L}\right)z = \frac{-2p^*_{1,0}x_0^k}{\rho L(L_T - L)^k} + \frac{2p^*_{atm}}{\rho L} - 2gsin\theta \tag{9}$$

It is observed that Equation (9) is a first-order linear differential equation with variable coefficients, where z is the unknown variable. Additionally, since the equation is non-homogeneous, its solution involves multiplying both sides by an integrating factor $e^{h(L)}$, where $h(L) = -\int \frac{f}{D} + \frac{2R_v g A^2}{s} ds$ is the integral of the second coefficient. Therefore, the integrating factor becomes

$$e^{h(L)} = e^{-\int \frac{f}{D} + \frac{2R_v g A^2}{s} ds} = e^{-\left(\frac{f}{D}\ L + 2R_v g A^2 (lnL)\ \right)} \tag{10}$$

Multiplying Equation (9) by the integrating factor in (10) yields the following result:

$$e^{h(L)}\frac{d(z)}{dL} - e^{h(L)}\left(\frac{f}{D} + \frac{2R_v g A^2}{L}\right)z = e^{h(L)}\left(\frac{-2p^*_{1,0}x_0^k}{\rho L(L_T - L)^k} + \frac{2p^*_{atm}}{\rho L} - 2gsin\theta\right) \tag{11}$$

By the definition of $h(L)$ and calculating $h\prime(L) = -\left(\frac{f}{D} + \frac{2R_v g A^2}{L}\right)$, the chain rule gives $\frac{d\left(e^{h(L)}\right)}{dL} = h'(L)e^{h(L)} = -\left(\frac{f}{D} + \frac{2R_v g A^2}{L}\right)e^{h(L)}$. This allows the left-hand side of Equation (11) to be rewritten using the product rule as follows:

$$\frac{d\left(ze^{h(L)}\right)}{dL} = e^{h(L)}\left(\frac{-2p^*_{1,0}x_0^k}{\rho L(L_T - L)^k} + \frac{2p^*_{atm}}{\rho L} - 2gsin\theta\right) \tag{12}$$

By integrating Equation (12) with limits from L_0 to L, where $v(L) > 0$, and $v(S) > 0$ for all S values, thus

$$ze^{h(L)} = \int_{L_0}^{L} \left(e^{(-\frac{f}{D}\ S)}(S)^{-2R_v g A^2}\right)\left(\frac{-2p^*_{1,0}x_0^k}{\rho S(L_T - S)^k} + \frac{2p^*_{atm}}{\rho S} - 2gsin\theta\right)dS \tag{13}$$

Dividing Equation (12) by Equation (10) yields

$$z = \left(e^{\frac{f}{D}\ L}(L)^{2R_v g A^2}\right)\int_{L_0}^{L} \left(e^{\frac{f}{D}\ S}(S)^{2R_v g A^2}\right)^{-1}\left(\frac{-2p^*_{1,0}x_0^k}{\rho S(L_T - S)^k} + \frac{2p^*_{atm}}{\rho S} - 2gsin\theta\right)dS \tag{14}$$

Considering that $z = v^2$, then the water velocity can be computed as

$$v(L) = \sqrt{\left(e^{\frac{f}{D}\ L}(L)^{2R_v g A^2}\right)\int_{L_0}^{L} \left(e^{\frac{f}{D}\ S}(S)^{2R_v g A^2}\right)^{-1}\left(\frac{-2p^*_{1,0}x_0^k}{\rho S(L_T - S)^k} + \frac{2p^*_{atm}}{\rho S} - 2gsin\theta\right)dS} \tag{15}$$

Equation (14) is valid for L values between L_0 and L_f, where $v(L) \geq 0$.

The solution of Equation (14) yields the integral of Equation (15).

$$\int_{L_0}^{L} \left(e^{\frac{f}{D}\ S}(S)^{2R_v g A^2} \right)^{-1} \left(\frac{-2p^*_{1,0}x_0^k}{\rho S(L_T - S)^k} + \frac{2p^*_{atm}}{\rho S} - 2gsin\theta \right) dS \tag{16}$$

Defining $\mathcal{M}(S)$ as the integrand of Equation (15), then

$$\mathcal{M}(S) = \left(e^{\frac{f}{D}S}(S)^{2R_v g A^2} \right)^{-1} \left(\frac{-2p^*_{1,0}x_0^k}{\rho S(L_T - S)^k} + \frac{2p^*_{atm}}{\rho S} - 2gsin\theta \right) \tag{17}$$

The function $\mathcal{M}(S)$ results in very small values that can cause an unstable solution, as demonstrated in Section 3.

In this sense, the average of the term $\left(e^{\frac{f}{D}\ L}(L)^{2R_v g A^2} \right)$ is selected for the solution.

$$z = \int_{L_0}^{L} \left(e^{\frac{f}{D}(L-S)} \left(\frac{L}{S} \right)^{2R_v g A^2} \right) \left(\frac{-2p^*_{1,0}x_0^k}{\rho S(L_T - S)^k} + \frac{2p^*_{atm}}{\rho S} - 2gsin\theta \right) dS \tag{18}$$

Denoting $\mathcal{N}(S)$ as the integrand of Equation (17) with $z = \int_{L_0}^{L} \mathcal{N}(S)dS$, then

$$\mathcal{N}(S) = \left(e^{\frac{f}{D}(L-S)} \left(\frac{L}{S} \right)^{2R_v g A^2} \right) \left(\frac{-2p^*_{1,0}x_0^k}{\rho S(L_T - S)^k} + \frac{2p^*_{atm}}{\rho S} - 2gsin\theta \right) \tag{19}$$

The resulting values of $\mathcal{N}(S)$ are bigger compared to $\mathcal{M}(S)$, yielding a reliable solution for emptying processes.

For the numerical solution of z, the Simpson's 1/3 rule with a fifth-order error was employed [20,21]. To approximate the integral of a function $\mathcal{N}(S)$ over the interval $[a, b]$, it is divided into n equal sub-intervals, each of length $h = \frac{b-a}{n}$. It is important to note that in Simpson's 1/3 rule, n must be an even number to ensure a suitable solution. By dividing the interval into n parts, the integral of $\mathcal{N}(S)$ for the values s_i with $i = 0, \ldots, n$, and considering that $z = \int_{L_0}^{L} \mathcal{N}(S)dS$ with $\mathcal{N}(S)$, then

$$\int_{L_0}^{L} \mathcal{N}(S)dS \approx (L - L_0) \frac{\mathcal{N}(L_0) + 4\sum_{i=0}^{\frac{n-2}{2}} \mathcal{N}(S_{2i+1}) + 2\sum_{i=1}^{\frac{n-2}{2}} \mathcal{N}(S_{2i}) + \mathcal{N}(L)}{3n} \tag{20}$$

The final solution is yielded by $v = \sqrt{-\int_{L}^{L_0} \mathcal{N}(S)dS}$.

3. Results

3.1. Dataset

This section shows the proposed approach's application. The model was developed to predict the minimum value of air pocket pressure pulses during an emptying procedure in a single installation. The proposed approach is applied to a water pipeline considering the dataset as follows: L_T = 350 m, k = 1.2, x_0 = 50 m, D = 0.25 m, f = 0.017, θ = 0.10 rad, and R_v = 0.15 ms^2/m^6. The Supplementary Materials section provides the code created using the proposed approach to model the emptying process, with calculations performed in Octave v7.1.0.

3.2. Application of the Proposed Approach

For a numerical resolution, a value of n = 30 was considered for the proposed approach. Figure 2 shows the obtained results that relate to the three analysed variables of the problem (water velocity, air pocket pressure, and length of the water column). The water velocity

starts with a null value, reaching a maximum of 4.77 m/s. The proposed approach predicts only the behaviour until the minimum value of the sub-atmospheric pressure head is 1.34 m. At this point, the water velocity once again reaches a zero value.

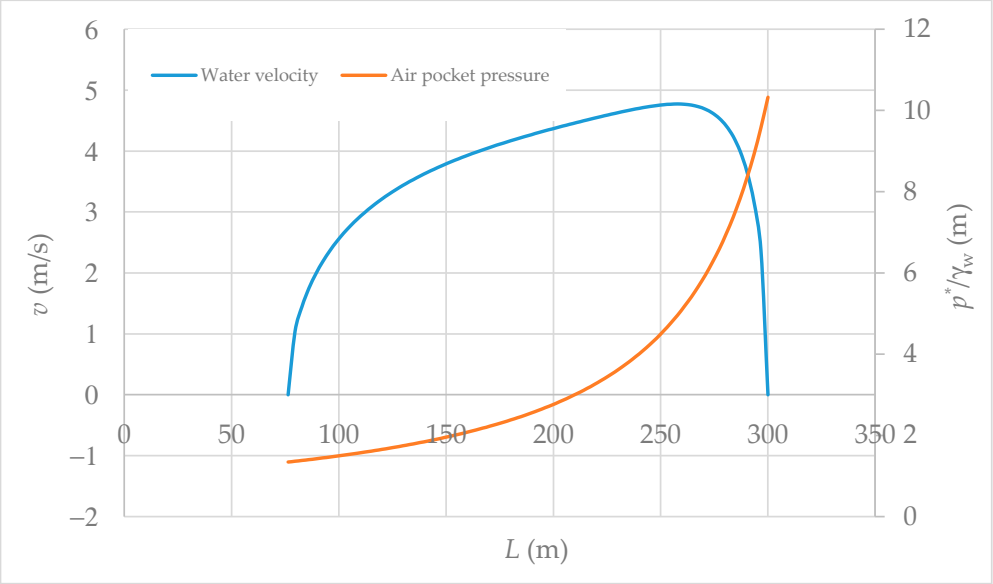

Figure 2. An analysis of hydraulic variables applying the proposed approach.

3.3. Effect of Main Parameters

The effects of the main parameters involved in this process are studied using the proposed approach. Figure 3 illustrates the relationship between the air pocket pressure head and the length of the water column, with variations in air pocket size. As expected, the smaller the air pocket size, the lower the values of sub-atmospheric pressure pulses achieved. In this instance, the air pocket size ranges from 10 to 150 m. An air pocket pressure of 0.205 m was found for an air pocket size of 10 m, while a value of 4.4 m was attained for a size of 150 m. It is paramount to remember that smaller air pocket sizes can lead to issues related to damaging pressure collapse depending on installation conditions and soil characteristics.

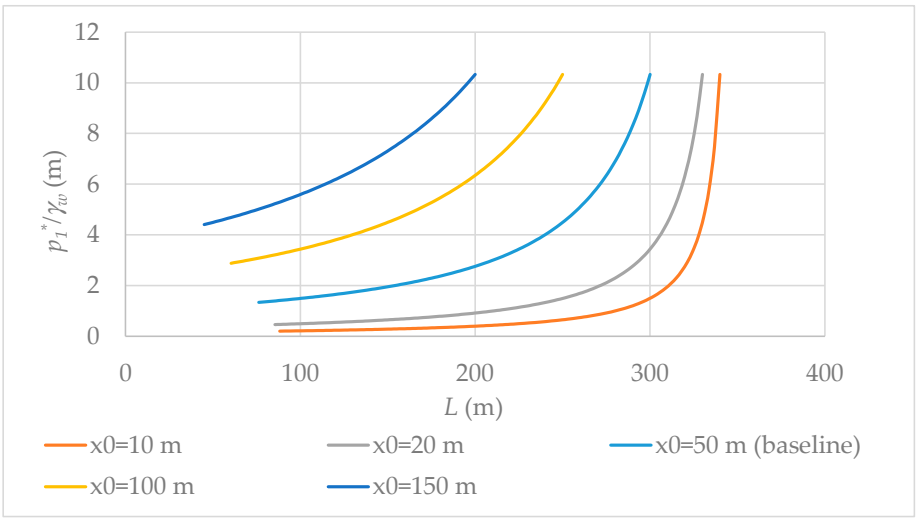

Figure 3. Relationship between air pocket pressure and water column length with varying air pocket sizes.

Another significant parameter is the selection of the polytropic coefficient. In practise, it is challenging to establish this coefficient a priori. During the design phase, engineers typically define an intermediate behaviour of the air phase (k = 1.2). The polytropic coefficient ranges between 1.0 (isothermal evolution) and 1.4 (adiabatic evolution). Figure 4 presents the minimum values of sub-atmospheric pressure heads against variations in the polytropic coefficient (k). Lower polytropic coefficients result in smaller sub-atmospheric pressure heads. However, there are no significant discrepancies across the entire range of the polytropic coefficient. In this sense, using k = 1.0, a minimum sub-atmospheric pressure of 1.31 m is obtained, while with k = 1.4, the air pressure reaches 1.37 m.

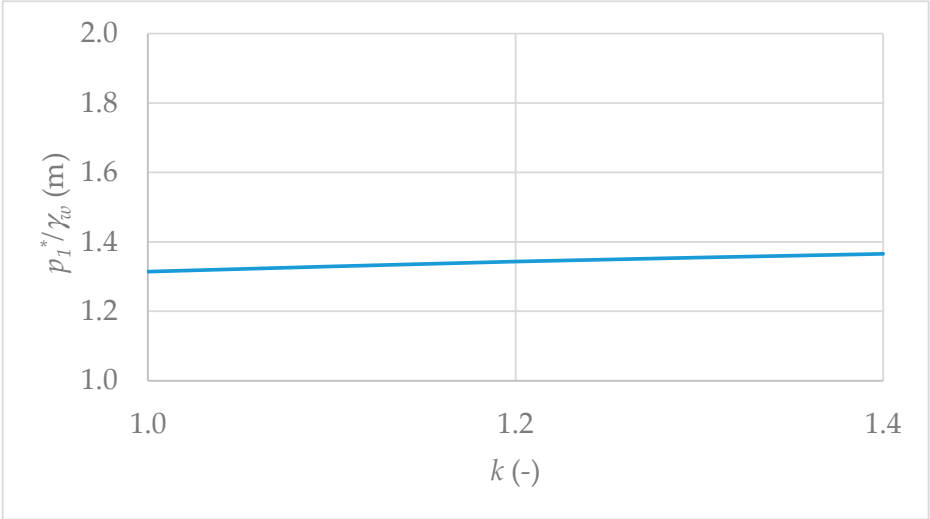

Figure 4. Minimum sub-atmospheric pressure heads as a function of the polytropic coefficient.

The internal pipe diameter was also varied to observe the behaviour of the proposed approach. Pipe diameters ranged between 0.15 and 0.40 m. No significant differences were detected when varying this parameter. For example, with a pipe diameter of 0.15 m, an air pocket pressure of 1.37 m is observed, whereas for a pipe diameter of 0.40 m, the air pocket pressure trends towards 1.31 m, as shown in Figure 5.

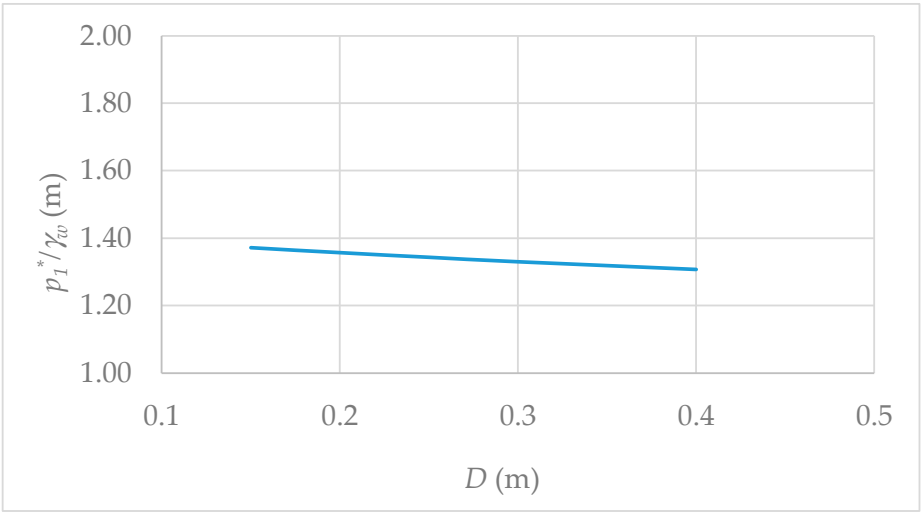

Figure 5. Variation in internal pipe diameter versus minimum sub-atmospheric pressure pulses.

Considering that the friction factor indicates how roughness can affect pipe resistance, various values ranging from 0.013 to 0.020 were analysed to observe the variations in

minimum sub-atmospheric pressure heads, as shown in Figure 6. The smaller the friction factor, the more significant the reduction in sub-atmospheric pressure. In this case, friction factor values of 0.013 and 0.020 resulted in minimum sub-atmospheric pressures of 1.32 and 1.35 m, respectively. This parameter does not significantly affect the phenomenon's behaviour during drainage events.

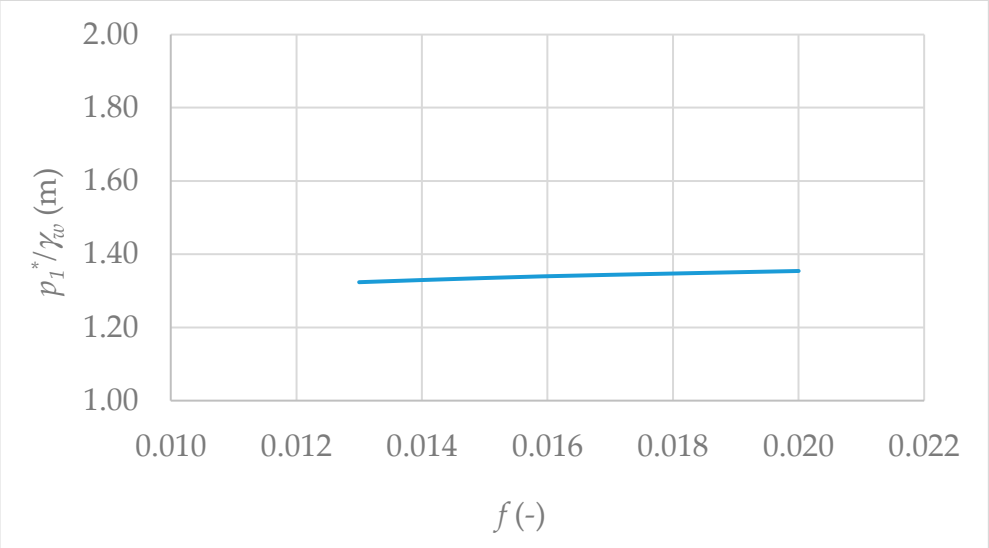

Figure 6. An analysis of the friction factor and its effect on the minimum sub-atmospheric pressure head.

Figure 7 analyses the variation in the resistance coefficient of a regulating valve, considering different aperture degrees ranging from 0.06 to 150 ms^2/m^6. The higher the resistance coefficient, the greater the air pocket pressure achieved, with values ranging from 1.34 to 1.38 m for the full range of analysed resistance coefficients.

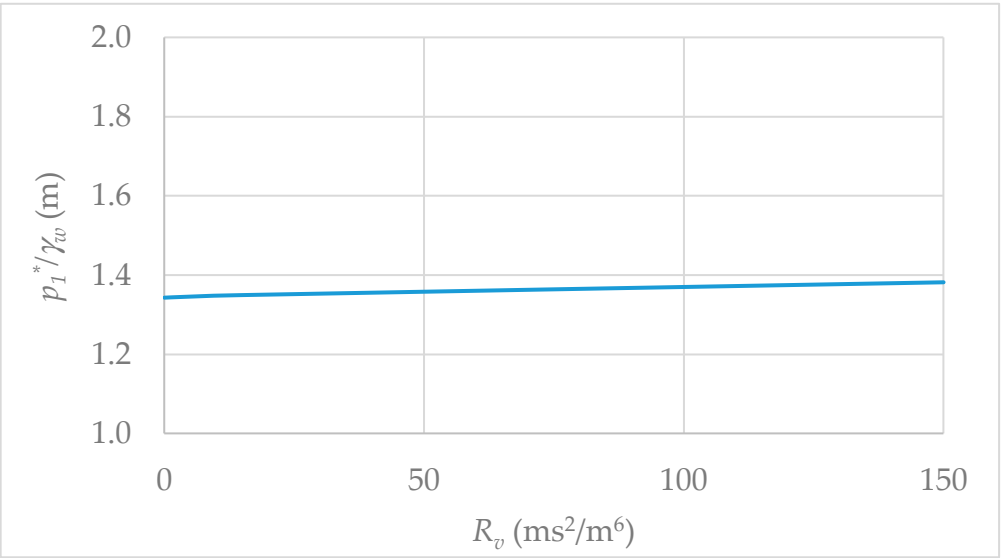

Figure 7. An analysis of the resistance coefficient of regulating valves on the minimum sub-atmospheric pressure heads.

As demonstrated in Figure 8, the bed slope significantly influences air pocket pressure pulses during emptying manoeuvres. To analyse these variations, pipe slopes from 0.05 to 0.20 radians were examined. The greater the bed slope, the lower the minimum sub-

atmospheric pressure heads attained. For instance, with a pipe slope (from 0.2 to 0.50 rad), a minimum pressure head of 1.96 m is reached, while a pipe slope of 0.20 rad results in a value of 1.13 m under the proposed approach.

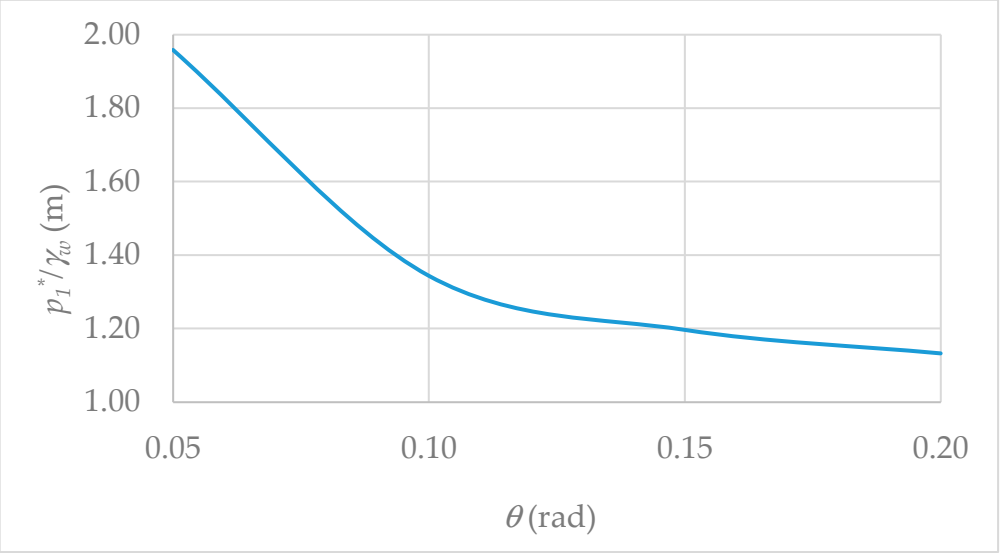

Figure 8. Influence of bed slope on minimum sub-atmospheric pressure heads.

4. Discussion

4.1. Numerical Resolution

A 1D mathematical model is compared to assess the proposed approach. The mathematical model is solved using Equations (1)–(3), which involve mass oscillation, piston flow, and polytropic formulations. These are based on physical formulations representing the emptying phenomena with entrapped air. The proposed approach uses these equations but only captures water movement until the minimum sub-atmospheric pressure occurs. As expected, both models exhibit the same behaviour, as illustrated in Figure 9. Indeed, the 1D mathematical model can replicate the transient event, but its numerical resolution is complex, as it involves a system of differential algebraic equations. The advantage of the proposed approach is that it offers a more straightforward numerical resolution.

Additionally, the results of Simpson's 1/3 rule approximation were compared with those of the trapezoidal rule, which has a third-order error, to evaluate the behaviour of the proposed approach. Both approximations yield reliable values for computing this process. For the interval $[s_i,\ s_{i+1}]$, the approximation of the trapezoidal rule for z is

$$\int_{L_0}^{L} \mathcal{N}(S)dS \approx \sum_{i=1}^{n} \left(\frac{L-L_0}{n}\right)\left(\frac{\mathcal{N}(S_{i-1})+\mathcal{N}(S_i)}{2}\right) \tag{21}$$

Since the numerical resolution requires the number of intervals (n) to be specified, both even and odd numbers were utilised to assess their influence on the numerical approach. In this regard, the numerical resolution was performed using values of 2, 3, 7, 8, 30 (baseline solution), and 35, as shown in Figure 10. Even numbers provided a better fit compared to odd numbers. The greater the selected value of n, the more accurate the solution for the proposed approach. For example, using an odd number of $n = 3$, the water column length is 86.04 m for a null water velocity (the instant when the minimum air pocket pressure is reached), whereas using an even number of $n = 4$ results in a value of 82.8 m. The even number is more closely aligned with the final behaviour of the process, where a value of 76.33 m was obtained for the baseline solution ($n = 30$).

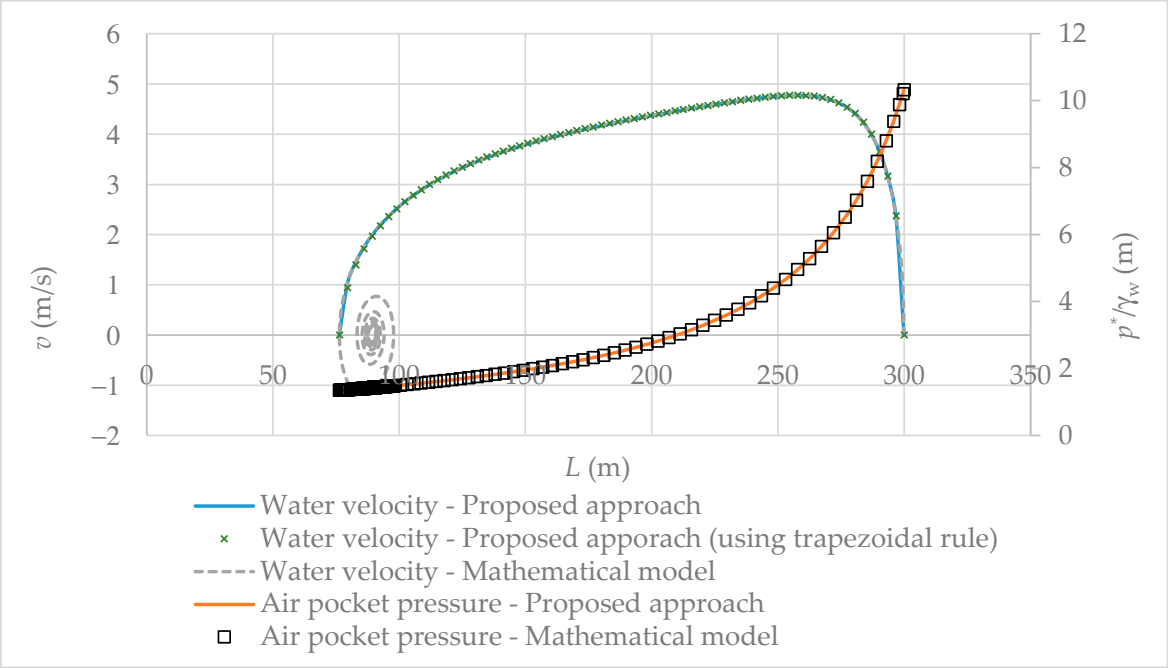

Figure 9. A comparison between the 1D mathematical model and the proposed approach.

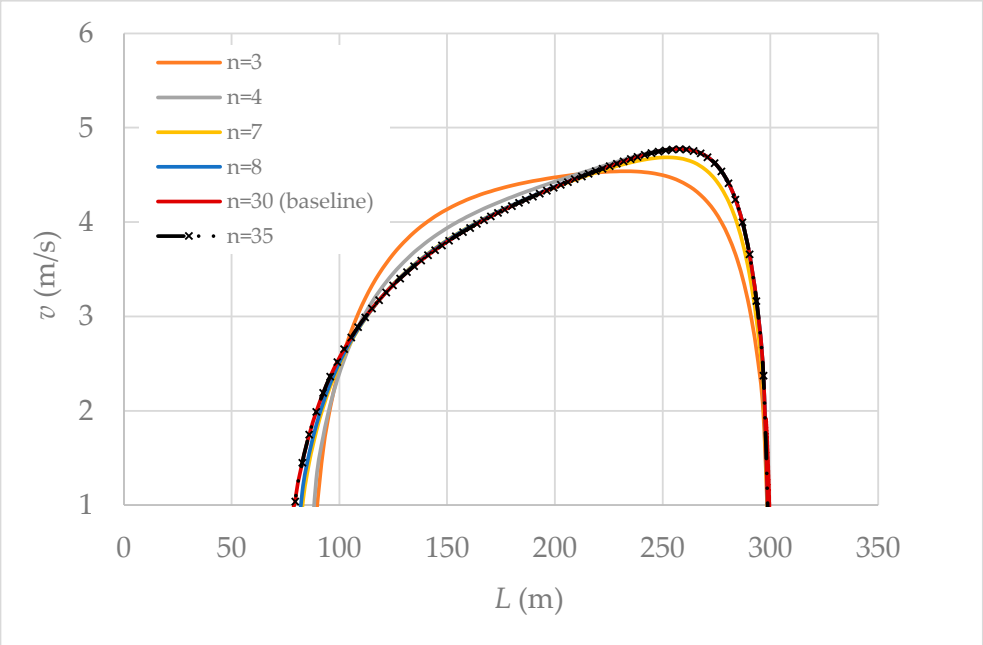

Figure 10. Variation in the number of intervals for numerical resolution.

The validation of the proposed approach also considers the assessment of $\mathcal{M}(S)$ and $\mathcal{N}(S)$, as shown in Figure 11. Figure 11a presents that the resulting $\mathcal{M}(S)$ values have a maximum in an order of magnitude around 10^{-4}, which is very small, and precision errors may arise during integration, causing the simulation to become unstable. In contrast, the $\mathcal{N}(S)$ values present a suitable value for integration purposes, as despicted in Figure 11b.

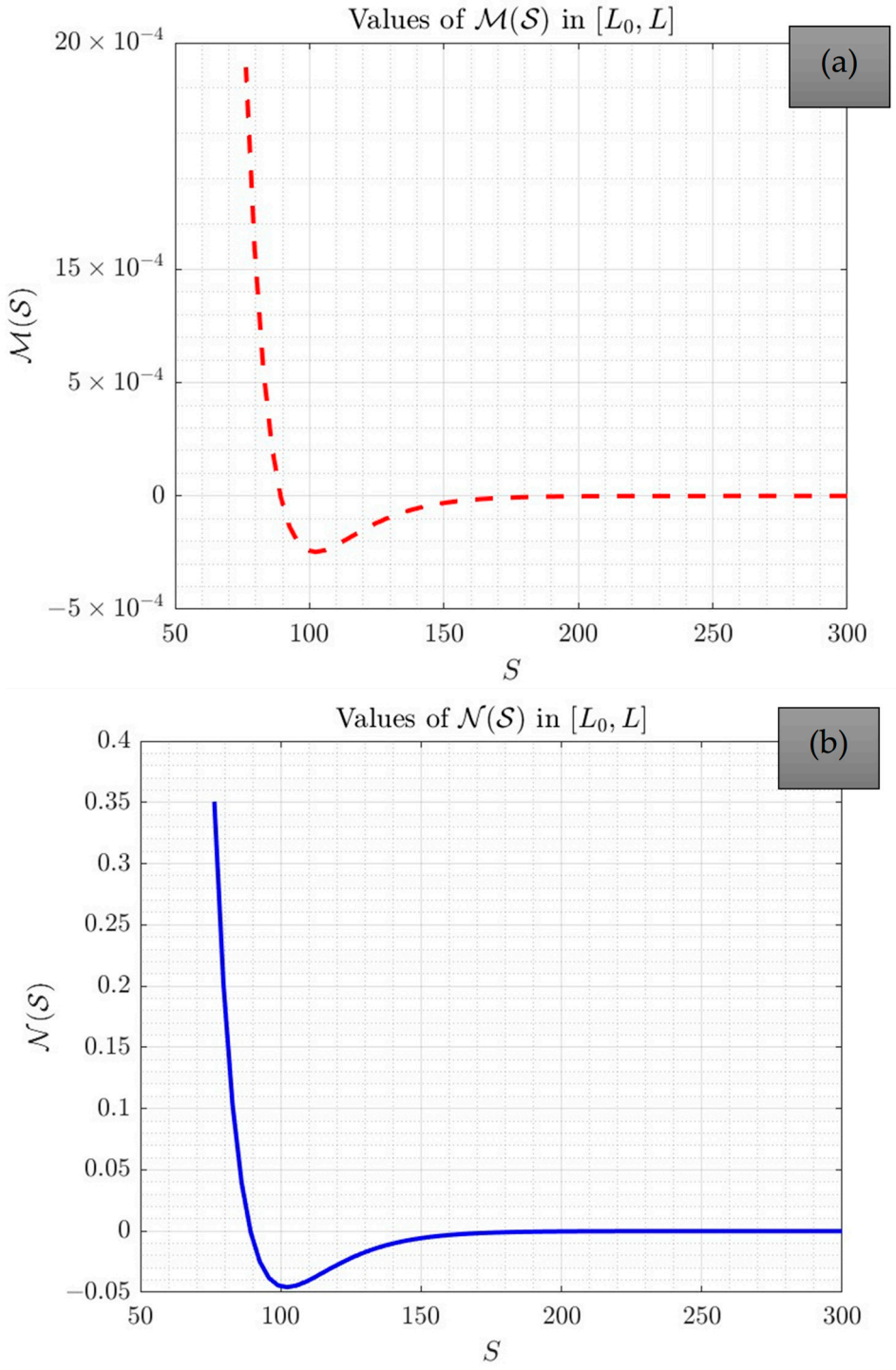

Figure 11. Computation of variables: (**a**) $\mathcal{M}(S)$; and (**b**) $\mathcal{N}(S)$.

4.2. Validation Employing Experimental Measurements

The proposed approach was validated using real-time measurements in a simple water pipeline, which the authors conducted. Data were obtained using a pressure transducer located at the highest point of the water installation, which consisted of a 4.36 m long pipe with an internal diameter of 42 mm. During the measurements, twelve (12) tests were carried out, varying the air pocket sizes from 0.205 to 0.450 m, with two slopes (0.457 and 0.515 rad) and employing opening manoeuvres in the regulating valve with resistance coefficients ranging from 11.89 to 138.41 ms^2/m^6. During the experiments, the opening

times of the regulating valve ranged from 0.15 to 0.75 s. Details of the experiments can be found in the publication conducted by Fuertes-Miquel et al. (2018).

The proposed approach considers an instantaneous opening of regulating valves, expected to yield sub-atmospheric pressure values lower than those observed in real-time experiments. This is significant, as the approach provides values that water utilities can use to plan emptying operations in real-world water installations. The proposed approach was validated by comparing the minimum sub-atmospheric pressure values obtained through real-time measurements. Additionally, both a one-dimensional (1D) mathematical model (comprising the numerical resolution of Equations (1)–(3)) and a three-dimensional (3D) CFD model were employed to simulate the current emptying operation.

Notably, for the current problem, the following equations are required:

Continuity equation:

$$\frac{\partial \rho}{\partial t} + \frac{\partial (\rho u)}{\partial x} + \frac{\partial (\rho v)}{\partial y} + \frac{\partial (\rho w)}{\partial z} = 0 \tag{22}$$

X-momentum equation:

$$\frac{\partial (\rho u)}{\partial t} + \frac{\partial \left(\rho u^2\right)}{\partial x} + \frac{\partial (\rho uv)}{\partial y} + \frac{\partial (\rho uw)}{\partial z} = -\frac{\partial p}{\partial x} + \frac{1}{R_{e,t}}\left[\frac{\partial \tau_{xx}}{\partial x} + \frac{\partial \tau_{xy}}{\partial y} + \frac{\partial \tau_{xz}}{\partial z}\right] \tag{23}$$

Y-momentum equation:

$$\frac{\partial (\rho v)}{\partial t} + \frac{\partial (\rho uv)}{\partial x} + \frac{\partial \left(\rho v^2\right)}{\partial y} + \frac{\partial (\rho vw)}{\partial z} = -\frac{\partial p}{\partial y} + \frac{1}{R_{e,t}}\left[\frac{\partial \tau_{xy}}{\partial x} + \frac{\partial \tau_{yy}}{\partial y} + \frac{\partial \tau_{yz}}{\partial z}\right] \tag{24}$$

Z-momentum equation:

$$\frac{\partial (\rho w)}{\partial t} + \frac{\partial (\rho uw)}{\partial x} + \frac{\partial (\rho vw)}{\partial y} + \frac{\partial \left(\rho w^2\right)}{\partial z} + = -\frac{\partial p}{\partial z} + \frac{1}{R_{e,t}}\left[\frac{\partial \tau_{xz}}{\partial x} + \frac{\partial \tau_{yz}}{\partial y} + \frac{\partial \tau_{zz}}{\partial z}\right] \tag{25}$$

Energy equation:

$$\begin{aligned} &\frac{\partial (E_T)}{\partial t} + \frac{\partial (uE_T)}{\partial x} + \frac{\partial (vE_T)}{\partial y} + \frac{\partial (wE_T)}{\partial z} \\ &\quad = -\frac{\partial (up)}{\partial x} - \frac{\partial (vp)}{\partial y} - \frac{\partial (wp)}{\partial z} - \frac{1}{R_{e,t}Pr_t}\left[\frac{\partial q_x}{\partial x} + \frac{\partial q_y}{\partial y} + \frac{\partial q_z}{\partial z}\right] \\ &\quad + \frac{1}{R_{e,t}}\left[\frac{\partial}{\partial x}\left(u\tau_{xx} + v\tau_{xy} + w\tau_{xz}\right) + \frac{\partial}{\partial y}\left(u\tau_{xy} + v\tau_{yy} + w\tau_{yz}\right) + \frac{\partial}{\partial z}\left(u\tau_{xz} + v\tau_{yz} + w\tau_{zz}\right)\right] \end{aligned} \tag{26}$$

where x, y, and z = tridimensional coordinate system; t = time; p = fluid pressure; ρ = fluid density; τ = fluid stress; q = heat flux; E_T = total energy of a fluid; $R_{e,t}$ = Reynolds number; u, v, and z = fluid velocity components in direction x, y, and z, respectively; and Pr_t = Prandtl number.

According to Paternina-Verona et al. (2023) [11], a 3D CFD model for emptying processes can be implemented based on the following assumptions: (i) non-isothermal and immiscible compressible flows; (ii) the air phase can be treated as an ideal gas; (iii) water density remains constant over time, as air elasticity is significantly higher compared to the water phase; and (iv) the pipe walls are modelled as rigid elements. The k-ω SST turbulence model was employed for the simulations, a model widely adopted by researchers to address air–water interface issues. Simulations were conducted using the OpenFOAM v2012 software with the compressibleInterFoam solver, which is well suited for modelling mixtures of air and water. For the calculations, the aspect ratio, non-orthogonality, and skewness were analysed across five meshes to validate the adopted 3D configuration.

The results of the 1D mathematical model and the 3D CFD model were compared to assess the proposed approach, as shown in Figure 12. As expected, the 1D mathematical model and 3D CFD model calibrated better than the proposed approach, since they are

based on physical formulations. However, applying the proposed approach is more accessible than these models. The 1D mathematical model requires a numerical resolution that involves ordinary differential equations, while the 3D CFD needs high computational times. The proposed approach is suitable for computing minimum values of air pocket pressure heads, being a practical tool that water utilities can use to predict rapidly emptying operations in actual water installations.

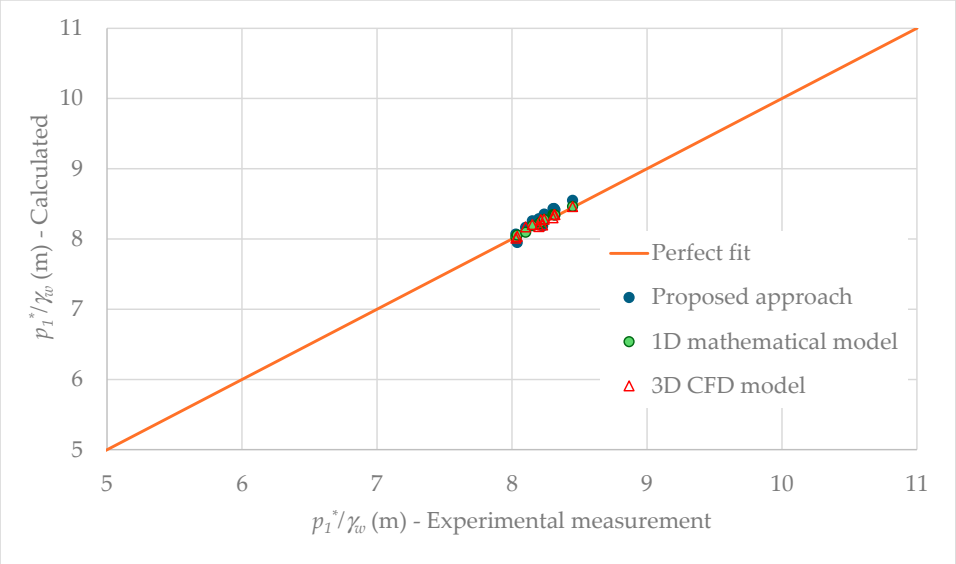

Figure 12. Minimum attained air pocket pressure heads for 1D and 3D models.

The root mean square error ($RMSE$) and the correlation coefficient were computed to assess the fit of the proposed approach numerically and its corresponding comparison with the 1D mathematical model and 3D CFD model, as presented in Table 1. It is essential to highlight that the proposed approach has good accuracy, with an $RMSE$ of 1.13% and an R^2 of 0.95. The used formulations are described as follows:

$$RMSE = \sqrt{\frac{1}{N}\sum_{j=1}^{N}\left(\frac{p^*_{1,cal} - p^*_{1,exp}}{p^*_{1,exp}}\right)^2} \tag{27}$$

$$R^2 = \frac{\sum_{j=1}^{N}\left(p^*_{1,cal,j} - \overline{p^*_{1,cal}}\right)\left(p^*_{1,exp,j} - \overline{p^*_{1,exp}}\right)}{\sqrt{\sum_{j=1}^{N}\left(p^*_{1,cal,j} - \overline{p^*_{1,cal}}\right)^2}\sqrt{\sum_{j=1}^{N}\left(p^*_{1,exp,j} - \overline{p^*_{1,exp}}\right)^2}} \tag{28}$$

where $RMSE$ = root mean square error; R^2 = correlation coefficient; $p^*_{1,cal}$ = air pocket pressure calculated using the proposed approach, 1D mathematical model, or 3D CFD model; $p^*_{1,exp}$ = experimental measurement; and N = total analysed points.

Table 1. Computation of root mean square errors and correlation coefficients.

Model	*RMSE* (%)	R^2
Proposed approach	1.13	0.95
1D mathematical model	0.33	0.99
3D CFD model	0.47	0.96

5. Conclusions

In this study, a new mathematical expression was developed to directly model the transient events in emptying operations within single water installations, including biphasic

flow. The mathematical approach was derived by solving the system of algebraic differential equations from the 1D model proposed by the authors. This method offers a more straightforward computational approach compared to previous models. The proposed approach was validated using an experimental facility with a pipe length of 4.36 m and an internal diameter of 42 mm. The mathematical approach can compute the minimum values of the sub-atmospheric air pocket pressure head with a root mean square error of 1.13%, slightly higher than the 1D mathematical model (0.33%) due to the consideration of instantaneous valve opening manoeuvres.

This research provides a foundation for water utilities to estimate the minimum sub-atmospheric air pressure pulses that may occur during emptying processes. Incorporating such expressions in digital twin models should be considered for predicting these phenomena. The proposed mathematical approach enables water utilities to select an appropriate pipe stiffness class based on soil characteristics and the drop in sub-atmospheric pressure pulses calculated by the model.

Supplementary Materials: The following supporting information can be downloaded at: https://www.mdpi.com/article/10.3390/w16223203/s1. This section includes the code programmed in Octave v7.1.0, which solved the emptying process for the dataset presented in Section 3.1.

Author Contributions: Conceptualization, D.M.B.-C. and O.E.C.-H.; methodology, D.M.B.-C., O.E.C.-H. and M.P.-S.; formal analysis, D.M.B.-C., A.A.-P., O.E.C.-H. and H.M.R.; writing—original draft preparation, A.A.-P., V.S.F.-M. and O.E.C.-H.; supervision, A.A.-P., V.S.F.-M. and H.M.R. All authors have read and agreed to the published version of the manuscript.

Funding: This research received no external funding.

Data Availability Statement: Data are contained within the article.

Conflicts of Interest: The authors declare no conflicts of interest.

References

1. Fuertes-Miquel, V.S.; Coronado-Hernández, O.E.; Iglesias-Rey, P.L.; Mora-Meliá, D. Transient Phenomena during the Emptying Process of a Single Pipe with Water–Air Interaction. *J. Hydraul. Res.* **2019**, *57*, 318–326. [CrossRef]
2. Tijsseling, A.S.; Hou, Q.; Bozkuş, Z.; Laanearu, J. Improved One-Dimensional Models for Rapid Emptying and Filling of Pipelines. *J. Press. Vessel. Technol.* **2015**, *138*, 31301. [CrossRef]
3. Laanearu, J.; Annus, I.; Koppel, T.; Bergant, A.; Vučković, S.; Hou, Q.; Tijsseling, A.S.; Anderson, A.; van't Westende, J.M.C. Emptying of Large-Scale Pipeline by Pressurized Air. *J. Hydraul. Eng.* **2012**, *138*, 1090–1100. [CrossRef]
4. Coronado-Hernández, O.E.; Fuertes-Miquel, V.S.; Besharat, M.; Ramos, H.M. Subatmospheric Pressure in a Water Draining Pipeline with an Air Pocket. *Urban Water J.* **2018**, *15*, 346–352. [CrossRef]
5. Chen, X.; Hou, Q.; Laanearu, J.; Tijsseling, A.S. Experimental Data on Filling and Emptying of a Large-Scale Pipeline. *Sci. Data* **2024**, *11*, 603. [CrossRef] [PubMed]
6. Baranovskii, E.S.; Burmasheva, N.V.; Prosviryakov, E.Y. Exact Solutions to the Navier–Stokes Equations with Couple Stresses. *Symmetry* **2021**, *13*, 1355. [CrossRef]
7. Tiwari, G.; Kumar, J.; Prasad, V.; Patel, V.K. Utility of CFD in the Design and Performance Analysis of Hydraulic Turbines—A Review. *Energy Rep.* **2020**, *6*, 2410–2429. [CrossRef]
8. Olsen, N.R.B. Three-Dimensional CFD Modeling of Self-Forming Meandering Channel. *J. Hydraul. Eng.* **2003**, *129*, 366–372. [CrossRef]
9. He, J.; Hou, Q.; Lian, J.; Tijsseling, A.S.; Bozkus, Z.; Laanearu, J.; Lin, L. Three-Dimensional CFD Analysis of Liquid Slug Acceleration and Impact in a Voided Pipeline with End Orifice. *Eng. Appl. Comput. Fluid Mech.* **2022**, *16*, 1444–1463. [CrossRef]
10. Liu, E.; Ma, X.; Zhou, M. Analysis of Discharge Process of Oil Pipeline with Complex Topography. *Energy Rep.* **2019**, *5*, 678–687. [CrossRef]
11. Paternina-Verona, D.A.; Coronado-Hernández, O.E.; Aguirre-Mendoza, A.M.; Espinoza-Román, H.G.; Fuertes-Miquel, V.S. Three-Dimensional Simulation of Transient Flows during the Emptying of Pipes with Entrapped Air. *J. Hydraul. Eng.* **2023**, *149*, 4023007. [CrossRef]
12. Chen, Y. *System Simulation Techniques with MATLAB and Simulink*; John Wiley & Sons: Hoboken, NJ, USA, 2013.
13. Eaton, J.W. *GNU Octave 4.2 Reference Manual*; Samurai Media Limited: Surrey, UK, 2017.
14. Madenci, E.; Guven, I. Fundamentals of ANSYS. In *The Finite Element Method and Applications in Engineering Using ANSYS®*; Springer: New York, NY, USA, 2006; pp. 15–35.

15. Chen, G.; Xiong, Q.; Morris, P.J.; Paterson, E.G.; Sergeev, A.; Wang, Y. OpenFOAM for Computational Fluid Dynamics. *Not. AMS* **2014**, *61*, 354–363. [CrossRef]
16. Hu, H.; Zhang, J.; Li, T. Dam-Break Flows: Comparison between Flow-3d, MIKE 3 FM, and Analytical Solutions with Experimental Data. *Appl. Sci.* **2018**, *8*, 2456. [CrossRef]
17. Chang, H.-C.; Noorizadegan, A.; Liu, Y.-H.; Ma, K.-T. A Study on Offshore Anchor Selection with a Focus on Torpe-do Anchor Stability and Performance. *J. Mar. Sci. Eng.* **2024**, *12*, 1721. [CrossRef]
18. Besharat, M.; Coronado-Hernández, O.E.; Fuertes-Miquel, V.S.; Viseu, M.T.; Ramos, H.M. Backflow Air and Pressure Analysis in Emptying a Pipeline Containing an Entrapped Air Pocket. *Urban Water J.* **2018**, *15*, 769–779. [CrossRef]
19. Zill, D.G. *Differential Equations with Boundary-Value Problems*; Cengage Learning: Boston, MA, USA, 2016.
20. Hoffman, J.D.; Frankel, S. *Numerical Methods for Engineers and Scientists*; CRC Press: Boca Raton, FL, USA, 2018.
21. Stoer, J.; Bulirsch, R.; Bartels, R.; Gautschi, W.; Witzgall, C. *Introduction to Numerical Analysis*; Springer: Berlin/Heidelberg, Germany, 1980; Volume 1993.